Medical Engineering and Physics 000 (2015) 1–6

Contents lists available at ScienceDirect

Medical Engineering and Physics

journal homepage: www.elsevier.com/locate/medengphy

Technical note

Colourimetric image analysis as a diagnostic tool in female genital schistosomiasis

Sigve Dhondup Holmen[a,b,*], Eyrun Floerecke Kjetland[a], Myra Taylor[c], Elisabeth Kleppa[a,b], Kristine Lillebø[a], Svein Gunnar Gundersen[a,d,e], Mathias Onsrud[b], Fritz Albregtsen[f,g]

[a] Centre for Imported and Tropical Diseases, Oslo University Hospital, Oslo, Norway
[b] Institute of Clinical Medicine, Faculty of Medicine, University of Oslo, Norway
[c] School of Public Health, Nelson Mandela School of Medicine, University of KwaZulu-Natal, South Africa
[d] Research Department, Sørlandet Hospital HF, Kristiansand, Norway
[e] Institute of Development Studies, University of Agder, Kristiansand, Norway
[f] Department of Informatics, University of Oslo, Oslo, Norway
[g] Institute for Cancer Genetics and Informatics, Oslo University Hospital, Oslo, Norway

ARTICLE INFO

Article history:
Received 27 May 2014
Revised 21 November 2014
Accepted 21 December 2014
Available online xxx

Keywords:
Female genital schistosomiasis
Diagnosis
Colposcopy
Cervix
Lesion
Colour

ABSTRACT

Female genital schistosomiasis (FGS) is a highly prevalent waterborne disease in some of the poorest areas of sub-Saharan Africa. Reliable and affordable diagnostics are unavailable. We explored colourimetric image analysis to identify the characteristic, yellow lesions caused by FGS. We found that the method may yield a sensitivity of 83% and a specificity of 73% in colposcopic images. The accuracy was also explored in images of simulated inferior quality, to assess the possibility of implementing such a method in simple, electronic devices. This represents the first step towards developing a safe and affordable aid in clinical diagnosis, allowing for a point-of-care approach.

Abbreviations

FGS	female genital schistosomiasis
HSV	Hue, saturation, value
RGB	red, green, blue
Lab	lightness, a and b
SNR	signal to noise ratio

1. Introduction

Female genital schistosomiasis (FGS) is a poverty-related disease caused by the water-transmitted parasite *Schistosoma haematobium*. The disease may create lesions and inflammation in the genital tract [1]. It is highly prevalent in certain rural areas of Africa, which have limited access to health care and diagnostics. The disease may cause vaginal bleeding, discomfort, dyspareunia, infertility and it might increase the risk of acquiring HIV [1–3].

The lesions associated with FGS consist of changes in the genital mucosa, the most characteristic being the sandy patches (Supplementary Figure 1). These may be classified in two subtypes: First, the sandy patches appearing as grains, which are pathognomonic of FGS [4]. They are characterised by yellow grains that appear clustered or singularly, both superficial and deep in the mucosa. Secondly, the sandy patches appearing as homogenous yellow areas, which are strongly associated with FGS [4].

Detection of ova in direct, bedside microscopy of crushed biopsies from lesions has been considered the gold standard in diagnosing FGS [1,5]. In an area endemic of HIV, biopsy may be considered a safe approach if sexual abstinence or condom protection can be assured one day prior to, and fourteen days following the procedure [6]. However, it is not possible to ensure that all patients follow these precautions, making biopsies an inappropriate diagnostic approach. Furthermore, pathology services are scarce and the transport of specimens (and patients for return visits) is often impossible. It is necessary to develop alternative methods for non-invasive, objective diagnosis of FGS that can be performed at the point of care [1].

Computerised image analysis has been applied in the classification of precancerous cervical lesions using both colour [7] and

* Corresponding author at: Institute of Clinical Medicine, University of Oslo, Postbox 1171 Blindern, 0316 Oslo, Norway. Tel.: +47 900 67 924.
E-mail address: sigve.holmen@medisin.uio.no (S.D. Holmen).

http://dx.doi.org/10.1016/j.medengphy.2014.12.007

Table 1
Exploring colour channels for differentiating the sandy patches from the adjacent mucosa.

Channel	$\bar{c}_{sandy\ patch}$	$\bar{c}_{mucosa}$	$\Delta_{\bar{c}}$	$\sigma\,\Delta_{\bar{c}}$	*t*-value	*p*-value	Reason for exclusion
Red	182.0	148.0	34.0	17.4	10.5	<0.001	
Green	111.4	82.0	29.3	16.0	9.9	<0.001	
Blue	107.3	89.7	17.7	17.0	5.6	<0.001	
Hue	114.6	177.3	7.4	5.6	7.2	<0.001	
Saturation	110.9	118.7	7.8	14.9	2.8	0.009	
Value	182.0	148.0	34.0	17.4	10.5	<0.001	
L	54.3	41.6	12.7	6.6	10.3	<0.001	Similar to *Value*
a	27.6	31.2	3.6	6.9	2.8	0.010	Significance level < 99.9%
b	14.8	7.5	7.30	7.9	5.0	<0.001	

$\bar{c}_{sandy\ patch}$: mean colour value of sandy patch;
$\bar{c}_{mucosa}$: mean colour value of adjacent mucosa;
$\Delta_{\bar{c}}$: difference of means between colours of sandy patches and adjacent mucosa;
$\sigma\,\Delta_{\bar{c}}$: standard deviation of $\Delta_{\bar{c}}$.
The *t*- and *p*-values were calculated using the Student's *t*-test.

texture analysis [8]. Automation of such algorithms has also been described [9]. This paper explores the possibility of exploiting the characteristic colour qualities of the sandy patches as a first step towards developing a computerised diagnostic tool for FGS. Camera equipped cell phones are widely available in developing countries [10], and this computerised image analysis could be implemented as a novel tool using that technology in the clinical diagnosis of FGS.

2. Material and methods

2.1. Image material

The images used to develop this method were acquired in a cross-sectional field study of young women (age 16–22 years) in Southern KwaZulu-Natal, South Africa. The area is endemic for urogenital schistosomiasis. The images were captured using an Olympus OCS-500 colposcope with a mounted Olympus E-420 10 megapixel (Mpx) single lens reflex device (SLR) or a Leisegang colposcope with a Canon EOS 40D 10 Mpx SLR. The image files were stored using high-quality JPEG compression along with data from the clinical investigation regarding lesion size, type, demarcation and location.

Thirty images with clearly visible sandy patches (as diagnosed by the investigating clinician at the time of the examination) were selected for training the computer algorithm. For the experimental validation, 60 images were randomly selected from other patients from the same geographical area: Half of the images from positive cases and half from negative cases (cases and controls). The controls were selected from those patients where sandy patches had not been found by colposcopy, ova had not been detected by microscopy of urine, schistosomal DNA had not been detected in neither cervico-vaginal lavage nor urine (by real time PCR), and no other pathology had been indicated. All the images included in this study fulfilled the following criteria: no foreign elements occluding the field of view (spatula, swab etc.), the lesion was visible within the field of view, there was no other dominant pathology.

2.2. Statistics

The difference in the mean colour values in each colour channel was evaluated using the Student's *t*-test.

The algorithm's read-out in pixels was recorded and used to plot a receiver operating characteristics (ROC) curve. The area under the curve (AUC) was calculated using SPSS Statistics v19 (SPSS Inc., NY, USA) and used as an indicator of the algorithm's predictive quality. The optimal cut-off level for defining a positive case was found by identifying the point on the ROC closest to the upper, left corner.

The significance relating to which imaging device and colposcope were used for capturing the images on the algorithm's output was evaluated using logistic regression using the state of the image (positive or negative) as the dependent variable.

2.3. Colour channels

There are a number of different colour-spaces and it may be difficult to predict which are most useful for a specific analysis [11]. In addition to the *RGB* colour-space, which was used when recording the images, we transformed the colours to the colour spaces called *HSV* and *CIE-Lab* using the open source image analysis software ImageJ (U.S. National Institutes of Health).

In order to train the algorithm in identifying the lesions based on colourimetric properties, the mean colour values were measured for each colour channel of the three selected colour-spaces in superficial grainy sandy patches and the adjacent, normal mucosa (see Table 1).

2.4. Identifying the region of interest

Colposcopic images may contain non-mucosal elements such as parts of the speculum, medical instruments and skin. This may complicate the image analysis. Automated detection of the region of interest (ROI) was performed, drawing from a previously described method [9]. The method exploits the fact that the cervix is characterised by colours in the tones of magenta and that it usually occupies the centre of the image. The colour channel *a* of the *Lab* colour space, represents the increasing intensity of magenta for increasing positive values. The ectocervical mucosa can therefore be characterised by high values of *a* in combination with a short distance from the centre of the image.

By creating a Cartesian coordinate system where the origin corresponds to the centre of the image (x = width/2 and y = height/2), a pixel's distance from the centre could be calculated using the Pythagorean Theorem. A two-dimensional representation of the image was then created using a pixel's distance from the centre of the image as the first dimension and the *a*-channel as the second dimension. The algorithm then identifies the cluster of pixels with the highest values of *a* combined with having the most central position (Fig. 1). The *a*-channel was first smoothed using a Gaussian blur filter with a radius of 35px to eliminate minor details. Clustering was done using the *k*-means method initialised with two points (seeds); closest to the upper left and lower right corners [9,12]. A binary mask was made from the largest group of connected pixels (4-neighbourhood) within the optimal cluster. Empirically, we set a lower threshold of the *a*-channel values corresponding to 65% of the range in order to not oversize the mask. This mask was represented on an empty canvas with the same dimensions as the original image and a 1:1 relationship of pixels. It served as a coarse indication of the ectocervix that had to be expanded in order to reach the ectocervical boundaries (Fig. 1).

Please cite this article as: S.D. Holmen et al., Colourimetric image analysis as a diagnostic tool in female genital schistosomiasis, Medical Engineering and Physics (2015), http://dx.doi.org/10.1016/j.medengphy.2014.12.007

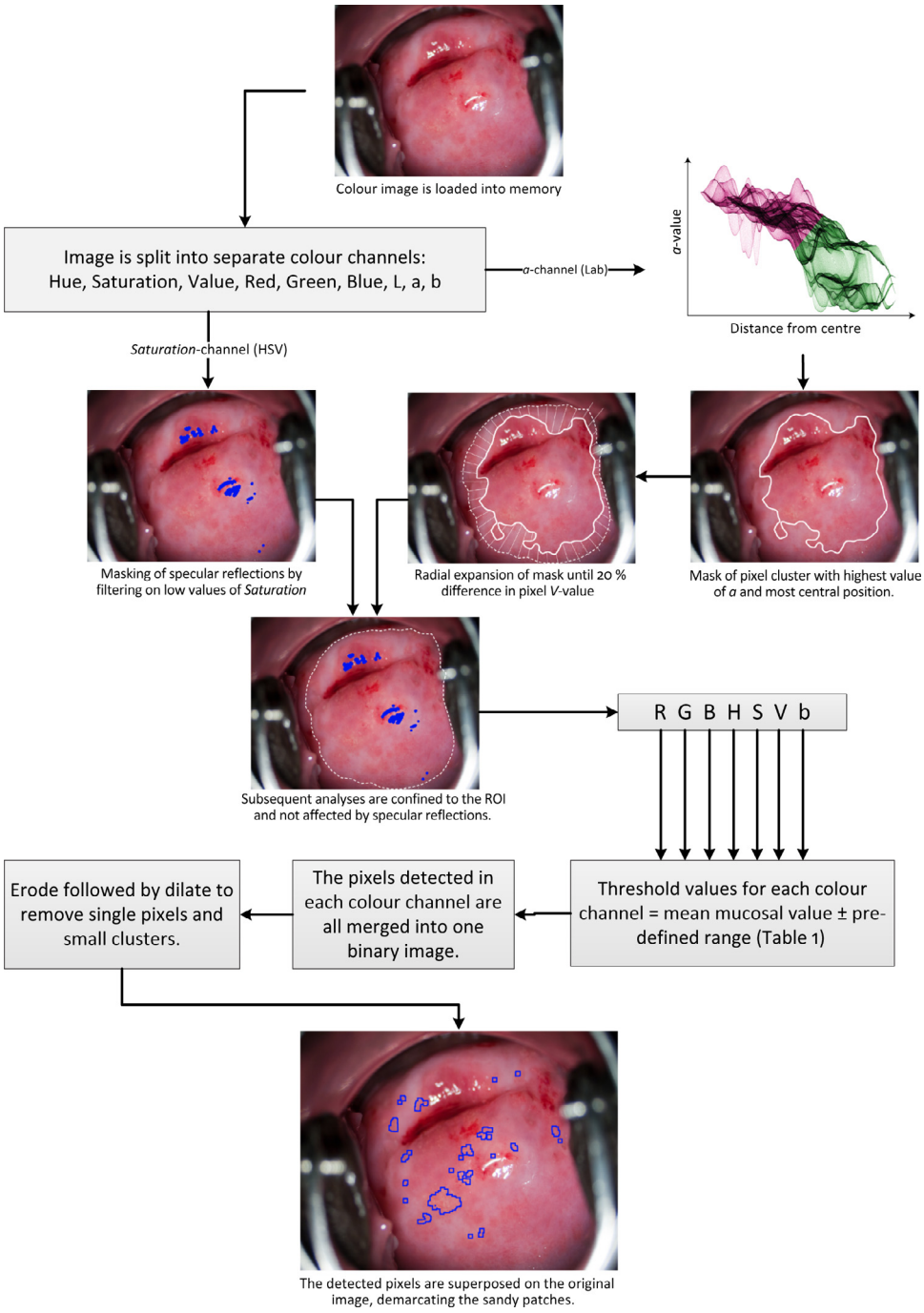

Fig. 1. Flow chart showing the steps of the algorithm. The original colour image is loaded into memory and then split into separate colour channels. Specular reflections are masked by filtering on low saturation in the saturation channel (HSV). Identification of the region of interest (ROI) consists of a coarse detection of the ectocervix by using the *a*-channel (Lab) and distance from the centre followed by radial growing, using the *Value*-channel (HSV). The adaptive thresholding is performed within the ROI, excluding the specular reflections, in each of the 7 colour channels. The binary results are joined by intersection, keeping only pixels present in all channels, followed by a morphological opening operation (see text). The final result is superposed on the original image, showing the algorithm's detection of sandy patches.

The delimitation of the ectocervix generally consists of a dark shade created by the mucosal fold between the convex ectocervix and the fornices. Expansion was therefore done by reading the pixel values of the *Value*-channel (of the *HSV* colour space) in 50 concentric rays originating from the centre of the coarse mask. Pixel values were only read peripheral to the mask area. A ray's end point was defined when a reduction in mean value of 20% or more for two consecutive runs of 50 pixels was found (i.e. 50 pixels were 20% darker than the former 50).

Finally a polygon was constructed by joining the end points of all the rays. To ensure a smooth delimitation of the ectocervix, the rays' lengths were smoothed by a 5-point mean filter. The resulting polygon defined the ROI for all subsequent analyses (Fig. 1).

2.5. Masking overexposed areas

Overexposed areas due to specular reflections from the mucosa represent artefacts that may perturb the image analysis. These areas were masked prior to analysis by filtering on low saturation using the *Saturation* channel (*HSV* colour space) [9]. The upper threshold value was defined adaptively as 1.5 standard deviations below the mean value of the analysed image's *Saturation* channel (with exceptions for

Please cite this article as: S.D. Holmen et al., Colourimetric image analysis as a diagnostic tool in female genital schistosomiasis, Medical Engineering and Physics (2015), http://dx.doi.org/10.1016/j.medengphy.2014.12.007

Table 2
Upper and lower threshold values for each colour channel.

Channel	Lower threshold	Upper threshold
Red	$\bar{x} + \Delta_{\bar{c}} - 2\sigma\,\Delta_{\bar{c}}$	$\bar{x} + \Delta_{\bar{c}} + 2\sigma\,\Delta_{\bar{c}}$
Green	$\bar{x} + \Delta_{\bar{c}} - 1.5\sigma\,\Delta_{\bar{c}}$	$\bar{x} + \Delta_{\bar{c}} + 2\sigma\,\Delta_{\bar{c}}$
Blue	x_{min}	$\bar{x} + \Delta_{\bar{c}} + 2\sigma\,\Delta_{\bar{c}}$
Hue	$\bar{x} + \Delta_{\bar{c}} - 0.625\sigma\,\Delta_{\bar{c}}$	$\bar{x} + \Delta_{\bar{c}} + 4\sigma\,\Delta_{\bar{c}}$
Saturation	$\bar{x} + \Delta_{\bar{c}} + 2\sigma\,\Delta_{\bar{c}}$	$\bar{x} + \Delta_{\bar{c}} + 2\sigma\,\Delta_{\bar{c}}$
Value	$\bar{x} + \Delta_{\bar{c}} - 2\sigma\,\Delta_{\bar{c}}$	$\bar{x} + \Delta_{\bar{c}} + 2\sigma\,\Delta_{\bar{c}}$
b	$\bar{x} + \Delta_{\bar{c}} - \sigma\,\Delta_{\bar{c}}$	x_{max}

The mean colour value ($\bar{x}$) is measured within the region of interest. The predicted colour value of a sandy patch corresponds to the addition of the previously calculated difference in colour values between sandy patches and healthy mucosa ($\Delta_{\bar{c}}$). The upper and lower values of the range are calculated by addition and subtraction, respectively, of various multiples of its standard deviation ($\sigma\,\Delta_{\bar{c}}$).

extreme values). The mask was expanded radially, adding a border of 20 pixels to ensure coverage of perimeter gradients (Fig. 1 and Supplementary Figure 2).

2.6. Adaptive detection of sandy patches

Images captured during colposcopy may vary in respect to exposure and colour [13] but the relative colour differences between healthy mucosa and sandy patches are fairly constant. This makes it possible to estimate a colour range that will most likely contain the sandy patches by measuring the mean mucosal colour value in each of the colour channels and adding the previously calculated difference of means between colours of sandy patches and adjacent mucosa for that particular channel (Table 1). The results represent the adaptive threshold values to be used to isolate the pixels of interest from each colour channel.

Table 2 shows that for most colour channels, the upper and lower limits of the range were defined by addition and subtraction of two standard deviations of the difference of the means, respectively, which approximates a 95% interval of confidence. For some channels, however, the expansion was based on knowledge of the colour channel's properties: e.g. the upper limit of the range for the channel *b* (of the *Lab* colour space) was always set to the maximum value because high values of *b* represent yellow colours. Likewise, the upper level of the *Hue*-channel was expanded by four standard deviations, as an increase in this channel's value represents a shift from tones of red to yellow. Using the lower and upper threshold values for each of the colour channels as given in Table 2, an adaptive thresholding is done in the 7 colour channels, and the binary results are merged to detect the sandy patches (Fig. 1).

To validate the algorithm's ability to adapt to different exposure levels, we created four images from a raw format image in the training set, changing the exposure levels to one and two units below (underexposure) and one and two units above (over-exposure) the original (correct) exposure. We then applied the colour analysis on all five images to compare how it performs with incorrect exposure.

2.7. Visual representation of detected pixels

The calculated ranges were used to set the upper and lower threshold limits in each of the colour channels, resulting in binary images, containing only pixels corresponding to the defined ranges. The binary images were then joined by intersection (keeping only pixels present in all the channels). The resulting binary image is then subject to a morphological opening operation: erosion followed by dilation, using a 3×3 pixel binary structuring element. The erosion removes small objects and details that the structuring element cannot fit inside, and shrinks all other objects. Dilating the result of the erosion with the same structuring element, the objects that survived the erosion will be restored.

Finally, the binary mask was translucently superimposed on the original colour image, showing the border between pathology (the sandy patch colour) and normal mucosa (Fig. 1), enabling visual verification of the result.

2.8. Simulating cheap, low-end imaging devices

The signal to noise ratio (SNR) was defined as the level of desired signal in the true digital image to the level of the noise occurring during image acquisition and compression, depending on hardware (lens, sensor) and software (image compression, noise filters). For reference purposes, we sought to measure the noise levels in two locally available devices of "high" and "medium" quality respectively: an 8 Mpx cell phone camera iPhone 4S (Apple Inc. 2011, Cupertino, USA) and a 2 Mpx Sony Ericsson w900i (Sony Ericsson 2005, Lund, Sweden). Measurement of noise was done by subtraction of ten pairs of identical images acquired in ambient light. By calculating the ratio of an 18% grey level to the standard deviation of the measured noise, the noise level may be expressed in a signal to noise ratio (SNR).

In order to simulate the inferior image quality expected from simple electronic devices, we created several lower quality versions of every image for the experimental validation. The images were scaled down to simulate a 5 Mpx camera (2738×1825 pixels) and random noise was added (ImageJ, U.S. National Institutes of Health), using a Gaussian distribution and standard deviations of 10 and 15 units, corresponding to SNRs at an 18% grey level of about 18 dB and 12 dB, respectively. For reference, the colposcopic cameras used for capturing the original images have been reported to produce SNRs in the range of 25–40 dB for ISO levels of 100–800 at an 18% grey level (DxO Labs, Boulogne, France).

3. Results

Table 1 shows the difference of the mean colour values calculated for each colour channel. The Hue channel was treated as a circular quantity (0–360°) when calculating the mean values. The difference of means was statistically different in all the colour channels. However, as the goal was to find the most useful colour channels, we chose to exclude the channel *a* in the step that detects the sandy patches, as it was the only colour channel with a significance level below 99.9%.

Several of the colour channels provide similar colour information, e.g. the channels *Value*, *L* and *Y* all represent a form of intensity of lightness. The algorithm would not benefit noticeably in terms of precision by including more than one colour channel per colour property. On the contrary, this would result in excessive processing requirements. As a consequence, for similar colour channels, we selected the ones with the highest level of significance as evaluated by the *t*-test (Table 1). This resulted in a model containing seven useful colour channels denoted *Red*, *Green*, *Blue*, *Hue*, *Saturation*, *Value* and *b* that were useful for differentiating the sandy patches from the surrounding mucosa. In addition, channel *a* was used together with *Saturation* and *Value* in order to establish the ROI within which the sandy patches were detected.

Fig. 2 shows the results of the ROC analyses for the two image sizes (10 and 5 Mpx) and different image qualities (artificially added noise). The respective AUCs are presented in Table 3. An optimal cut-off value for the full-resolution images was found to be 40,000 pixels, using the point on the ROC curve closest to the upper left corner. The cross-table for the full-resolution outcome is presented in Supplementary Table 1. The positive predictive value was calculated to be 76% and the negative predictive value was 81%.

The type of imaging device and colposcope that was used to capture the images did not affect the output significantly ($p = 0.41$).

Supplementary Figure 3 shows that the algorithm's adaptive approach allows it to correctly identify the lesions even with as much as two units of underexposure and one unit of overexposure.

Please cite this article as: S.D. Holmen et al., Colourimetric image analysis as a diagnostic tool in female genital schistosomiasis, Medical Engineering and Physics (2015), http://dx.doi.org/10.1016/j.medengphy.2014.12.007

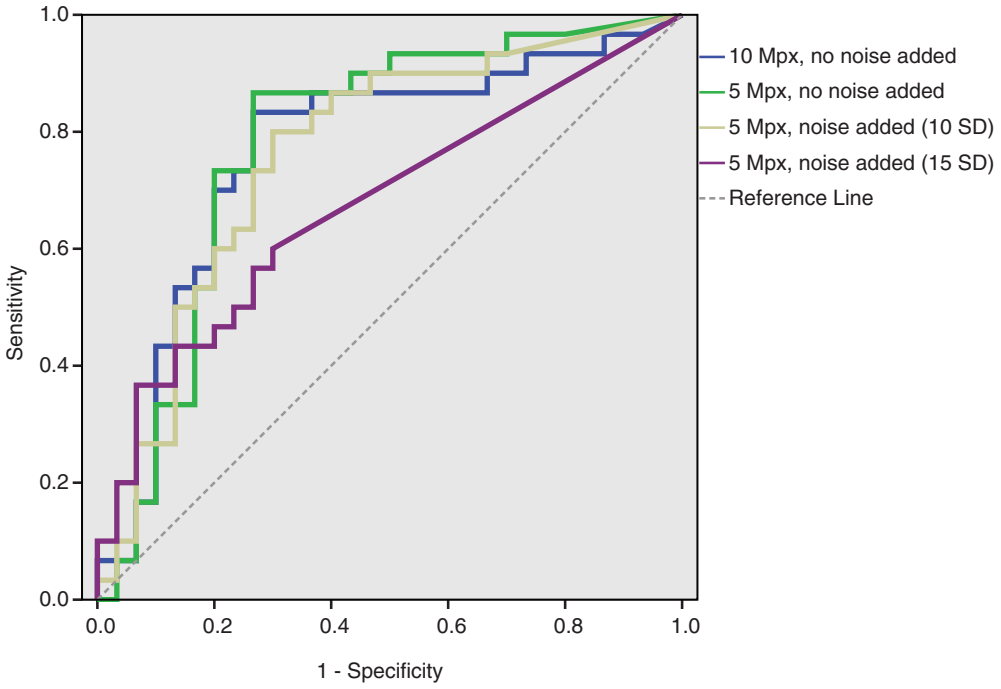

Fig. 2. Receiver operating characteristics (ROC) curves for the different image sizes and qualities.

Table 3
Simulating low-end imaging devices.

Quality	AUC[a]	Sensitivity	Specificity
10 Mpx, no noise added	0.77	83%	73%
5 Mpx, no noise added	0.78	87%	73%
5 Mpx, noise added (10 SD)[b]	0.76	80%	70%
5 Mpx, noise added (15 SD)[b]	0.67	60%	70%

[a] Area under receiver operating characteristics curve.
[b] Noise was generated using a Gaussian distribution with 10 or 15 standard deviations.

The noise levels produced by the low-end cameras were measured to a mean of 25.9 dB and 26.4 dB for the iPhone 4S and Sony Ericsson w900i, respectively. This is in the lower range of the SNRs produced by the SLRs used in this study, but in the upper range of the simulated noise that was added to the images.

4. Discussion

The algorithm presented in this paper was written as a Java-plugin for ImageJ and allowed unsupervised, automated analysis of batches of images. It was able to detect ectocervical sandy patches in FGS by colour analysis. It applies an adaptive thresholding technique in which the mean mucosal colour value in each image is measured and used as a reference value to calculate an appropriate threshold range per colour channel. This allows for a greater flexibility in exposure and colour balance. Artefacts were excluded automatically by defining a region of interest (ROI) and masking reflections.

This computer colour analysis represents a first step towards developing a computerised diagnostic tool. A computerised algorithm may be implemented in electronic devices such as mobile phones or laptops [14] allowing for deployment in developing countries where it may provide an affordable point of care diagnosis without the need for medical expertise. It may also provide a useful aid in the clinical diagnosis, improving on objectivity and inter-observer variability.

A Botswanan study showed that currently available cell phones are equipped with camera technology adequate for use in lieu of colposcopes for tele-medical screening of cervical cancer [15]. Mobile phone cameras have also been found to be adequate for tele-diagnostic purposes using manual computerised image analysis [16].

4.1. Strengths

The algorithm's adaptive feature allows variation in image exposure with as much as 2 units of underexposure. It also allows for some degree of overexposure, but we found that with 2 units of overexposure, there is not enough colour information left in the image to perform the colour analysis, as shown in Supplementary Figure 3.

The choice of method for refining the initial mask to a final ROI was largely based on the requirement of keeping the processing power to a minimum due to future implementation in mobile devices. By reading pixel values in only a limited number of rays, the processing power required is equally limited.

4.2. Limitations

Poor focus will be a problem for smaller patches and grains, as they become confluent with the surrounding mucosa. For clusters and larger patches, poor focus has little consequence for the colourimetric diagnosis.

The gradients around the perimeter of mucosal and specular reflections may mimic the colour qualities of sandy patches. This problem can be bypassed by masking the reflections. Several methods have been described for automated detection and such masking, either filtering high brightness and low saturation or by morphological top hat filtration [9,17]. We found that a simple filter on low saturation followed by expansion of the mask was adequate. However, when applying such a filter, the masked areas become unavailable for the analysis. This increases the likelihood of under-diagnosis with the size of the masked area and the size of the mask should there for be kept as small as possible.

4.3. Future research

The presented algorithm relies solely on lesion colour. Although it shows promising results for the identification of sandy patches,

the performance is not sufficient to be used as a diagnostic tool by itself. It is necessary to enhance the ability to distinguish FGS from other pathology such as cell atypia or sexually transmitted infections (STI). Grainy sandy patches have a distinct granular appearance of relatively constant size and aspect ratio that may render them suitable for texture analysis. Furthermore, the convoluted vessels that are significantly associated with sandy patches should be explored for morphological feature analysis [4]. The precancerous stages of cervical cancer may present with other distinct vascular patterns and several methods of texture analysis have been described for the latter [8,18,19] making it possible for an algorithm aimed at diagnosing genital schistosomiasis to draw from this in order to prevent misdiagnosis.

5. Conclusion

We found that an adaptive, colourimetric method of image analysis combined with automated image pre-processing can detect lesions caused by FGS with a sensitivity of 83% and a specificity of 73%. This represents the first step towards developing an automated diagnostic algorithm for a neglected tropical disease, for which there are currently no safe and cheap diagnostic possibilities in endemic areas. If implemented in simple, electronic devices, a diagnosis based on image analysis could represent an affordable diagnostic alternative in areas where other diagnostic possibilities are limited by resources and availability.

Ethical considerations

This project is part of a larger scientific study that was granted permissions by four ethics committees: the Biomedical Research Ethics Administration, University of KwaZulu-Natal in 2011 (BF029/07), the Department of Health, Pietermaritzburg, KwaZulu-Natal in 2009 (HRKM010-08), the Norwegian ethics committee of Eastern Norway in 2007 (469-07066a1.2007.535) and The European Group on Ethics in Science and New Technologies in 2011 (IRSES-2010:269245). The Provincial and District Departments of Health and Education in Ugu district, KwaZulu-Natal have also given permissions.

Written informed consent was obtained from all participants. They were informed of their right to withdraw from the study and examinations at any moment. The participants received treatment or referral for conditions that were diagnosed during the investigations.

Conflict of interest

None.

Acknowledgements

We would like to thank the staff at our research clinic, without whom this study would not have been possible.

Supplementary materials

Supplementary material associated with this article can be found, in the online version, at doi:10.1016/j.medengphy.2014.12.007.

References

[1] Kjetland EF, Leutscher PDC, Ndhlovu PD. A review of female genital schistosomiasis. Trends Parasitol 2012;28(2):58–65.
[2] Downs JA, Mguta C, Kaatano GM, Mitchell KB, Bang H, Simplice H, et al. Urogenital schistosomiasis in women of reproductive age in Tanzania's Lake Victoria region. Am J Trop Med Hyg 2011;84(3):364–9.
[3] Kjetland EF, Ndhlovu PD, Gomo E, Mduluza T, Midzi N, Gwanzura L, et al. Association between genital schistosomiasis and HIV in rural Zimbabwean women. AIDS 2006;20(4):593–600.
[4] Kjetland EF, Ndhlovu PD, Mduluza T, Gomo E, Gwanzura L, Mason P, et al. Simple clinical manifestations of genital Schistosoma haematobium infection in rural Zimbabwean women. Am J Trop Med Hyg 2005;72(3):311–19.
[5] Poggensee G, Sahebali S, Van Marck E, Swai B, Krantz I, Feldmeier H. Diagnosis of genital cervical schistosomiasis: comparison of cytological, histopathological and parasitological examination. Am J Trop Med Hyg 2001;65(3):233–6.
[6] Hasselrot K, Cheruiyot J, Kimani J, Ball TB, Kaul R, Hirbod T. Feasibility and safety of cervical biopsy sampling for mucosal immune studies in female sex workers from Nairobi, Kenya. PloS one 2012;7(10):e47570.
[7] Pogue BW, Mycek MA, Harper D. Image analysis for discrimination of cervical neoplasia. J Biomed Opt 2000;5(1):72–82.
[8] Ji Q, Engel J, Craine E. Texture analysis for classification of cervix lesions. IEEE Trans Med Imaging 2000;19(11):1144–9.
[9] Greenspan H, Gordon S, Zimmerman G, Lotenberg S, Jeronimo J, Antani S, et al. Automatic detection of anatomical landmarks in uterine cervix images. IEEE Trans Med Imaging 2009;28(3):454–68.
[10] Etzo S, Collender G. The mobile phone 'revolution' in Africa: rhetoric or reality?. Afr Aff 2010;109(437):659–68.
[11] Stokman H, Gevers T. Selection and fusion of colour models for image feature detection. IEEE Trans Pattern Anal Mach Intell 2007;29(3):371–81.
[12] Macqueen J. Some methods for classification and analysis of multivariate observations Proceedings of the fifth Berkeley symposium on mathematical statistics and probability et al. California, USA 1967. p. 281–97.
[13] Alush A, Greenspan H, Goldberger J. Automated and interactive lesion detection and segmentation in uterine cervix images. IEEE Trans Med Imaging 2010;29(2):488–501.
[14] Ballagas R, Borchers J, Rohs M, Sheridan J. The smart phone: a ubiquitous input device. IEEE Pervasive Comput 2006;5(1):70–7.
[15] Quinley KE, Gormley RH, Ratcliffe SJ, Shih T, Szep Z, Steiner A, et al. Use of mobile telemedicine for cervical cancer screening. J Telemed Telecare 2011;17(4):203–9.
[16] Martinez AW, Phillips ST, Carrilho E, Thomas III SW, Sindi H, Whitesides GM. Simple telemedicine for developing regions: camera phones and paper-based microfluidic devices for real-time, off-site diagnosis. Anal Chem 2008;80(10):3699–707.
[17] Lange H. Automatic glare removal in reflectance imagery of the uterine cervix *Proceedings of SPIE medical imaging*, vol. 5747 2005. p. 2183–92.
[18] Dickman ED, Doll TJ, Chiu CK, Ferris DG. Identification of cervical neoplasia using a simulation of human vision. J Low Genit Tract Dis 2001;5(3):144–52.
[19] Srinivasan Y, Corona E, Nutter B, Mitra S, Bhattacharya S. A unified model-based image analysis framework for automated detection of precancerous lesions in digitized uterine cervix images. IEEE J Select Top Signal Process 2009;3(1):101–11.